Multiband and Low-Specific-Absorption-Rate Wearable Antenna With Low Profile Based on Highly Conductive Graphene Assembled Film

Yang Xiao, Haoran Zu, Rongguo Song, Yitong Xin, Yueyue Xi, Guan-Long Huang, *Senior Member, IEEE*, Bian Wu, *Senior Member, IEEE*, and Daping He

***Abstract*—A flexible tri-band antenna with low profile and low specific absorption rate (SAR) based on highly conductive graphene assembled film (GAF) is proposed. The antenna incorporates GAF with polydimethylsiloxane to provide the flexibility for wearable applications. To reduce the effect of backward radiation on human body, a new multiband artificial magnetic conductor (AMC) reflector is proposed, which consists of several circular patches. The measured operating bandwidths of GAF antenna include 2.26–2.46 GHz (WiFi band), 3.52–3.68 GHz (5G n77 band), and 4.94–5.26 GHz (5G WLAN band). Correspondingly, the realized gain varies from 5.7–7.9 dBi. The proposed GAF antenna shows good flexibility and radiation stability when loaded on human body. The simulated SAR peak value is 0.51 W/kg at 2.36 GHz, 0.61 W/kg at 3.6 GHz, and 0.562 W/kg at 5.1 GHz when the tissue is 1 g, which meets the international standard. All results demonstrate that the proposed flexible GAF tri-band antenna is suitable for integrating in wireless wearable communication system.**

***Index Terms*—Flexible tri-band antenna, graphene assembled film (GAF), low specific absorption rate (SAR), tri-band artificial magnetic conductor, wearable antenna.**

I. Introduction

THE latest wireless and mobile communication technologies have been rapidly changing and developing to meet the increasing demands of intelligent communication, medical treatment and military, where flexible and low-profile wearable antennas have played a significant role [1], [2], [3]. Furthermore, in an effort to reduce coupling between antennas, reduce the size of communication systems, and improve the problem of electromagnetism, dual-band/multiband antennas have generated great concern among researchers [4], [5], [6].

In recent years, research on wearable antennas has continued to focus on the following three central issues: conformal ability, performance on the human body, and the necessity of reducing the value of specific absorption rate (SAR) [7], [8]. In the era of innovative electronic systems, an essential way of realizing the flexibility of wearable antennas is through a change in the conductive material. Various intelligent textiles can be used for wearable antennas, which provide high flexibility and have been sewn into clothing using textile materials [9], [10], [11], [12], such as conductive cotton fabric [13], taffeta, and nylon. However, the textile materials often easily appear cracks with human mechanical movement, deteriorating the performance of antenna [14], [15]. With the development of science and technology, there has been increasing interest in new conductive materials, such as conductive foils [16] and conductive ink [17], which can be easily incorporated into polymers to improve mechanical strength. Nevertheless, low electrical conductivity is a nonnegligible shortcoming. For the last few years, graphene-based film has been widely used in the antenna design field due to its high metal-matching conductivity, flexibility, mechanical stability, and other advantages [18], [19]. Many works design antennas with graphene film as the conductive material, such as ultra-wideband antennas [20], antenna array [21] and soft dual-band antennas [22], et al. As far as we know, the technology for developing graphene film to demonstrate and realize tri-band wearable antennas has not been reported before, not to mention the combination of low SAR and low profile, which are the crucial indexes for wearable antennas [23], [24], [25], [26], [27]. To sum up, it still come to a significant problem to propose a graphene assembled film (GAF) multiband wearable antenna with a low-profile structure and low SAR for wearable on/off-body communication.

In this letter, we propose a tri-band conformal antenna based on GAF with a high specific conductance of 1.1×10^6 S/m. With the excellent flexibility and mechanical stability benefited from the GAF, the wearable antenna achieves three operating bands of 2.26–2.46, 3.52–3.68, and 4.94–5.26 GHz. The measured maximum realized gain of the GAF antenna is 7.9 dBi. It can be seen that the GAF antenna maintains good performance under different bending conditions and stable work on human body from the measured results. With the advantages of low profile, good flexibility, and low SAR, the GAF tri-band antenna provides the superiorities for wearable applications and the on/off-body network communication.

Manuscript received 6 April 2023; revised 3 May 2023 and 24 May 2023; accepted 26 May 2023. Date of publication 30 May 2023; date of current version 6 September 2023. This work was supported in part by the National Natural Science Foundation of China under Grant 51672204, Grant 51701146, and Grant 62001338 and in part by the Fundamental Research Funds for the Central Universities under Grant WUT: 2020IB005, Grant 205209016, and Grant 2019IB017. *(Yang Xiao and Haoran Zu contributed equally to this work.) (Corresponding author: Daping He.)*

Yang Xiao, Haoran Zu, Rongguo Song, Yitong Xin, Yueyue Xi, and Daping He are with the Hubei Engineering Research Center of RF-Microwave Technology and Application, Wuhan University of Technology, Wuhan 430070, China (e-mail: 261206@whut.edu.cn; zuhr@foxmail.com; rongguo_song@whut.edu.cn; xinyitong@whut.edu.cn; huiyueyue12@foxmail.com; hedaping@whut.edu.cn).

Guan-Long Huang is with Foshan University, Foshan 528225, China (e-mail: hgl@fosu.edu.cn).

Bian Wu is with the National Key Laboratory of Antennas and Microwave Technology, Xidian University, Xi'an 710071, China (e-mail: bwu@mail.xidian.edu.cn).

Digital Object Identifier 10.1109/LAWP.2023.3281395

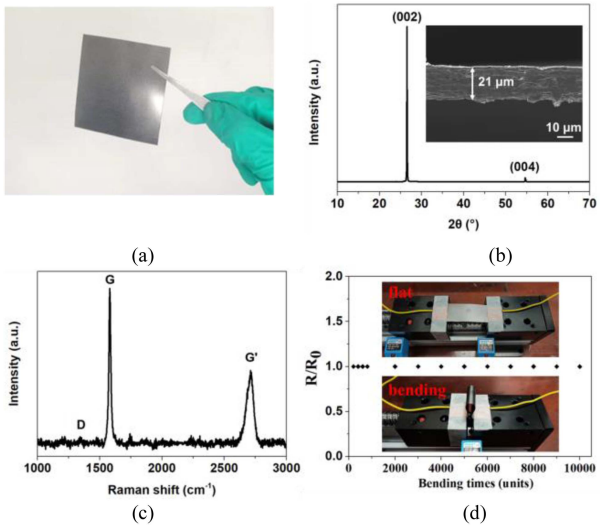

Fig. 1. (a) Digital photograph of GAF. (b) XRD pattern of GAF. (c) Raman spectrum of GAF. (d) Experiment of mechanical reliability of GAF sample.

II. Characterization of the GAF

The graphene-assembled film has shown a bright development prospect in the realm of wearable applications with its excellent flexibility, mechanical reliability, and chemical stability, which are fabricated in our previous works [28], [29]. Fig. 1(a) shows the digital photograph of the GAF sample. Since the electronic conductivity of GAF (1.1×10^6 S/m) is very close to the electrical conductivity of metal, this provides a great possibility in antenna design. Fig. 1(b) shows the cross-sectional SEM image of GAF, showing that the thickness of GAF is around 21 μm. The steepest graphitic peak (002) in the GAF's X-ray diffraction (XRD) pattern, which is positioned at 26.5°, is evidence that the graphene nano-sheets are stacked regularly in the GAF. Additionally, the distinctive peak (004) shows a significant degree of graphitization in the GAF. Moreover, Fig. 1(c) shows the Raman spectrum of GAF. The very strong G peak with the negligible D peak demonstrates that the GAF has almost no defects. As shown in Fig. 1(d), the experiment of mechanical reliability of GAF sample is exhibited. The GAF can stay in the same state after 10 000 bends and maintain unchanged resistivity, which can prove its mechanical stability and flexibility. Thus, the flexible, fatigue-resistant and highly conductive GAF is suitable for flexible wearable antenna design.

III. Mechanism of Antenna Design

A. Antenna Design

Fig. 2(a) demonstrating a monopole antenna with single band is proposed. The next step is Fig. 2(b), L-shape resonant branch is added to the radiant patch. It aims to realize miniaturization and achieve dual operating bands. On top of Fig. 2(b), a new F-shaped branch is added to the antenna in Fig. 2(c), which aims to realize three working bands. The final proposed antenna consists of three patches of different shapes and two rectangular grounds in Fig. 2(d), which are made of GAF. The GAF antenna is fabricated on a flexible polydimethylsiloxane (PDMS) (ε_r= 2.7, tan σ = 0.013) substrate with a thickness (H_1) of 1 mm. The overall size of the antenna ($W \times L$) is 20 mm × 30 mm. Fig. 2(e) shows the variation of $|S_{11}|$ from antenna 1 to antenna

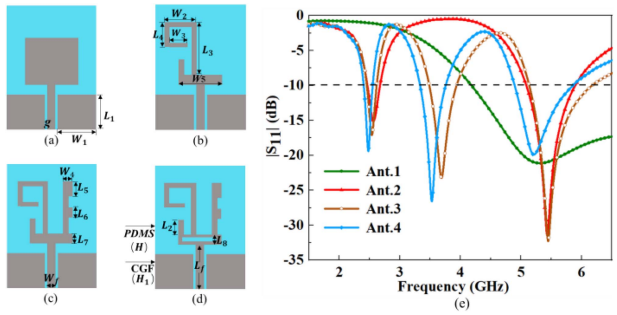

Fig. 2. (a)–(d) Process of antenna design. (e) Return loss of antenna 1 to antenna 4.

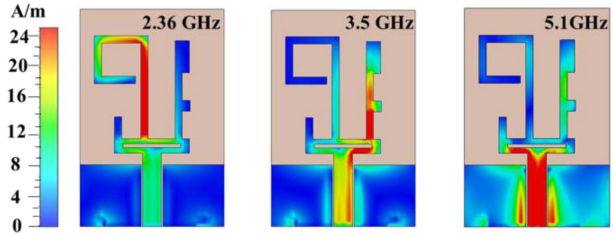

Fig. 3. Simulated surface current distribution at resonant frequencies: 2.36, 3.6, and 5.1 GHz.

TABLE I
Structural Parameters of the Proposed Wearable Antenna

Parameter	H	H_1	W_1	W_2	W_3	W_4	W_5	g
Value (mm)	1	0.025	8.7	6.25	3.2	2.0	10.4	0.2
Parameter	W_f	L_1	L_2	L_3	L_4	L_5	L_6	L_7
Value (mm)	2.56	8.5	3	14	5.6	3.2	2.2	2
Parameter	L_8	R_6	R_5	R_4	R_3	R_2	R_1	L_f
Value (mm)	0.5	13.8	11.8	10.5	8.5	8	5.2	10

4. The further miniaturization is attained by etching slots in the rectangular distribution and increases the capacitance effect. The surface current distribution shown in Fig. 3 can better reflect the resonances at different frequencies of the antenna design. From these two figures, it can be obviously observed that the low (2.36 GHz) and high (5.1 GHz) resonances are excited by the left branch and the main monopole radiator, and the middle resonance (3.6 GHz) is generated by adding the right branch. Additional impedance matching and resonance tuning are realized by etching a slot on the main monopole radiator, which can help adjust the current distribution for the monopole antenna. The structural parameters of the proposed antenna are shown in Table I.

B. Antenna AMC-Backed Design

Artificial magnetic conductors (AMCs) have been widely studied since they were proposed, and they have become a fast-growing research topic in many fields. AMC's reflection rule arises from its surface impedance changing with the resonant frequency. As the incident electromagnetic waves come into contact with the AMC surface, they form a high-impedance surface at the designed frequency band [23]. When the antenna's

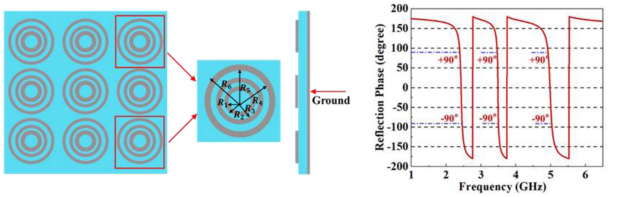

(a) (b)

Fig. 4. (a) 3 × 3 AMC reflection array and the parameters of the unit cell. (b) Diagram of the phase of reflection.

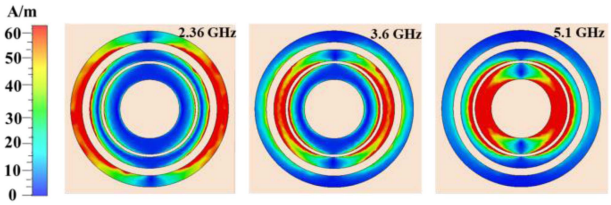

Fig. 5. Simulated surface current distribution at 2.36, 3.6, and 5.1 GHz.

resonant frequency matches the band gap of the reflective phase of AMC, it will reflect electromagnetic waves with the phase. It has the same amplitude with incident wave [30], [31]. It can improve the antenna gain and other radiation characteristics.

Based on the design principle of the AMC array, a circular GAF-AMC structure with three in-phase reflection phase bands is designed for the tri-band monopole antenna mentioned in the previous section. The proposed tri-band wearable AMC reflector is configured with 3 × 3 unit cells. The AMC structure is deployed on PDMS with a thickness of 2 mm and an overall size of 90 × 90 × 2 mm^3, which are shown in Fig. 4(a). An important parameter of the AMC structure is the reflection phase. In this letter, the reflection phase of −90 to 90° is considered in phase with the incident wave, which means the phase of the incident wave is −90 to 90°. In other words, the reflection phase of −90 to 90° calibrates the multiple operating bands of the proposed AMC structure. Therefore, the reflection phase of the AMC structure is shown in Fig. 4(b). The result indicates that the operating bandwidths of the reflection phase are 2.34–2.56, 3.42–3.58, and 4.86–5.14 GHz, which can match the bandwidths of the tri-band antenna.

Fig. 5 shows the surface current distribution at three different resonant frequencies, which can better explain the relation of different ring patches to the zero reflection phase. It can be seen that different radii of the rings determine the different working frequencies.

IV. Antenna Comparison on Open Space and Human Body

The antenna proposed in this letter is placed on a 3 × 3 AMC array as presented in Fig. 6(a). It shows that a foam is placed between the monopole antenna and the AMC reflector for supporting. The single antenna and the antenna loaded with AMC array are measured by the vector network analyzer. The simulated and measured reflection coefficients of integrated design in free space are shown in Fig. 6(b). The results show that the antenna with new-designed AMC reflector effectively operates in three frequency bands of 2.36, 3.6, and 5.1 GHz

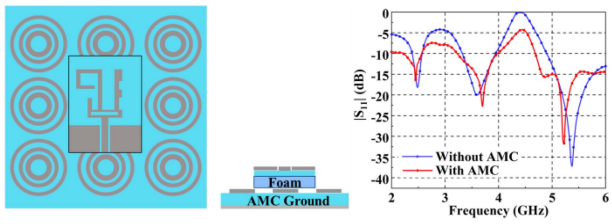

(a) (b)

Fig. 6. (a) Simulation schematic diagram. (b) Measured $|S_{11}|$ of the monopole antenna without and with AMC reflector.

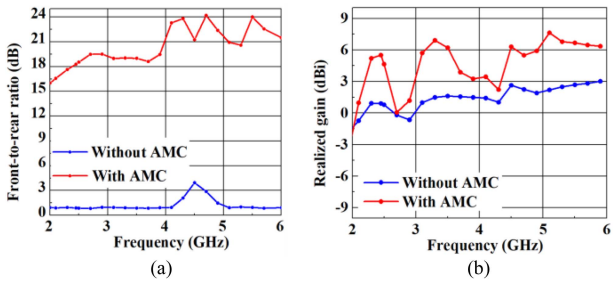

(a) (b)

Fig. 7. (a) Result of the front-to-back ratio of the antenna without and with AMC reflector. (b) Measured realized gain of the antenna without and with AMC reflector.

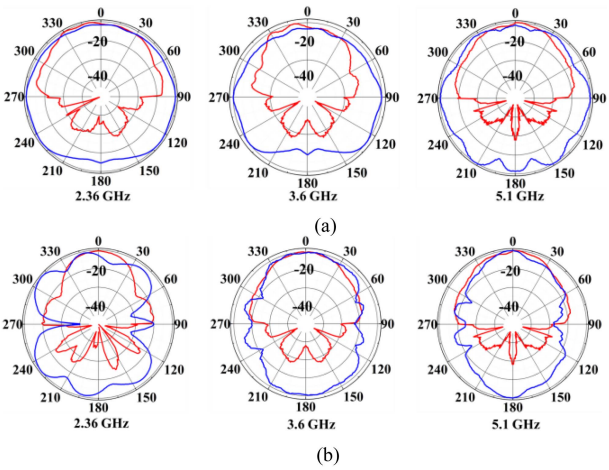

Fig. 8. Measured results of the normalized radiation pattern with AMC (red line) and without AMC (blue line). (a) *X-Z* plane. (b) *Y-Z* plane.

with bandwidths of 8.2%, 6.87%, and 7.5%, respectively. The antenna with AMC array can sufficiently reduce the backward radiation and positive radiation and front-to-back ratio as shown in Fig. 7(a). Fig. 7(b) shows the comparison of measured realized gain, which resulted in a higher realized gain of 5, 5.5, and 6 dBi at different operating frequencies bands. Fig. 8(a) and (b) shows the comparison of normalized radiation patterns between the monopole antenna without and with the AMC reflector. As observed, the AMC array plays a significant role in improving directivity of antenna and reducing effect of backward radiation.

V. Fabrication and Measurements of Antenna

After optimizing the simulation, laser engraving method is used to fabricate the GAF antenna based on the designed model

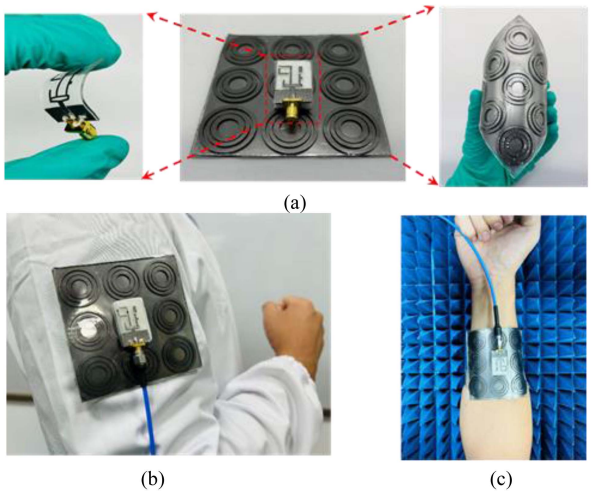

Fig. 9. (a) Photographs of the GAF wearable antenna. (b) Photograph of antenna loaded on the cloth. (c) Photograph of antenna loaded on the arm.

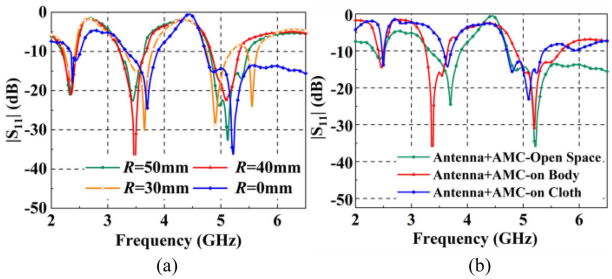

Fig. 10. (a) Measured $|S_{11}|$with different bending radii (R). (b) Measured $|S_{11}|$at different wearing conditions.

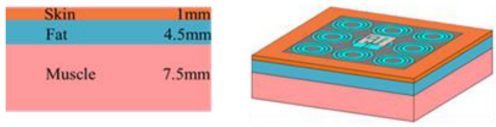

Fig. 11. Simulation for SAR of proposed antenna.

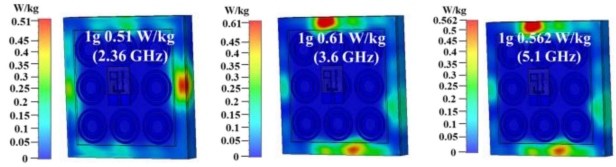

Fig. 12. Simulated SAR distribution of the wearable antenna.

TABLE II
COMPARISON OF SIGNIFICANT WORKS IN WEARABLE ANTENNA FIELD

Ref.	Size (λ_0*λ_0)	Profile (mm)	Operating bands	Gain (dBi)	SAR (W/kg)
[10]	0.83* 0.83	4.6	Single band	10.1	1.56
[14]	1.2*1.2	4.0	Single band	4.26	> 1.6
[15]	1.7* 1.1	5.1	Single band	6.12	N.A
[23]	0.87* 0.87	10.2	Dual-band	4.5/6.1	1.25
[25]	0.7*0.7	6.1	Dual-band	9/7.3	0.76
This work	0.68* 0.68	3.34	Tri-band	5.7/7.2/ 7.9	0.51/0.61/ 0.56

[29]. The GAF and PDMS are composited by resin adhesive. The practical photograph of the antenna is shown in Fig. 9(a). After fabrication, we set the antenna on different conditions, as shown in Fig. 9(a)–(c), which aims to model the human body on the different cases. Fig. 10(a) reflects that the reflection coefficients of different bending radii remain below −10 dB within the resonance of three working bands (2.26–2.46, 3.52–3.68, and 4.94–5.26 GHz). The reason for the frequency deviation is that the foam plate can not make a synchronous bend when the structure has a sharp bend. Nonetheless, the antenna can cover the required resonant bands with various bending radii. Fig. 10(b) shows measured $|S_{11}|$ in open air space and directly attached to the human body and cloth. The result reveals that the middle and high-frequency bands have a frequency offset. Even so, the proposed antenna can still work stably in the designed three frequency bands. In conclusion, the GAF antenna shows good flexibility and stable radiation properties for wearable applications.

Wearable antennas should be competent for on-body applications. Thus, the wearing safety of the proposed wearable antenna needs to be taken into consideration. The model is used to simulate the human tissue (skin, fat, and muscle), which has a size of $90 \times 90 \times 13$ mm^3. The antenna model loaded on human body is shown in Fig. 11, and some simulated parameters of human body are given in [20] and [26]. The SAR generally represents the rate of absorption of electromagnetic energy by human tissue, which is generally described in units of W/kg. IEEE C95.1 stipulates that the maximum absorption value should be less than 1.6 W/kg of 1 g tissue on the human body. CST Microwave Studio is used to calculate SAR values. As depicted in Fig. 12, the result shows that the maximum SAR level at three different frequencies are 0.51, 0.61, and 0.56 W/kg, respectively, all results are less than 1.6 W/kg, which accord with the international standard.

A comparison of the GAF wearable antenna with other works is listed in Table II. Compared with other wearable antennas with low SAR, the proposed GAF tri-band wearable antenna covers more frequency bands with low profile, and has good flexibility and mechanical properties. In addition, the proposed GAF wearable antenna shows a lower SAR value.

VI. CONCLUSION

A flexible GAF tri-band CPW-feed monopole wearable antenna is designed, fabricated, and measured. The GAF wearable antenna has only 3.34 mm profile and the operating bands cover 2.26–2.46, 3.52–3.68, and 4.94–5.26 GHz, including WiFi/5G n77/5G WLAN bands. Moreover, the GAF antenna has several mechanical benefits, including tremendous flexibility and consistent radiation performance. Incorporating the designed multiband AMC reflector structure, the GAF antenna achieves a high realized gain of 5–7.9 dBi over the three working bands. Furthermore, the SAR values of the antenna are under 1.6 W/kg, which is in accordance with the IEEE International Standard. Therefore, the GAF wearable antenna shows superiorities for on/off-body communication.

REFERENCES

[1] A. K. Yetisen, J. L. Martinez-Hurtado, B. Ünal, A. Khademhosseini, and H. Butt, "Wearables in medicine," *Adv. Mater.*, vol. 30, pp. 1706910–1706915, 2018.

[2] M. Yuan, R. Das, E. McGlynn, R. Ghannam, Q. H. Abbasi, and H. Heidari, "Wireless communication and power harvesting in wearable contact lens sensors," *IEEE Sensors J.*, vol. 21, no. 11, pp. 12484–12497, Jun. 2021.

[3] P. Okas, A. Sharma, and R. K. Gangwar, "Grounded CPW multi-band wearable antenna for MBAN and WLAN applications," *Microw. Opt. Technol. Lett.*, vol. 60, pp. 561–568, 2017.

[4] H. Yang, Y. Fan, and X. Liu, "A compact dual-band stacked patch antenna with dual circular polarizations for beidou navigation satellite systems," *IEEE Antennas Wireless Propag. Lett.*, vol. 18, no. 7, pp. 1472–1476, Jul. 2019.

[5] W. Liu, K. Zhang, J. Li, and S. Yan, "A wearable tri-band half-mode substrate integrated waveguide antenna," *IEEE Antennas Wireless Propag. Lett.*, vol. 20, no. 12, pp. 2501–2505, Dec. 2021.

[6] T. T. Le and T.-Y. Yun, "Miniaturisation of a dual-band wearable antenna for WBAN applications," *IEEE Antennas Wireless Propag. Lett.*, vol. 19, no. 8, pp. 1452–1456, Aug. 2020.

[7] N. A. Malik, P. Sant, T. Ajmal, and M. Ur-Rehman, "Implantable antennas for bio-medical applications," *IEEE J. Electromagn., RF Microw. Med. Biol.*, vol. 5, no. 1, pp. 84–96, Mar. 2021.

[8] T. Liang and Y. J. Yuan, "Wearable medical monitoring systems based on wireless networks: A review," *IEEE Sensors J.*, vol. 16, no. 23, pp. 8186–8199, Dec. 2016.

[9] M. E. Lajevardi and M. Kamyab, "Ultraminiaturized metamaterial-inspired SIW textile antenna for off-body applications," *IEEE Antennas Wireless Propag. Lett.*, vol. 16, pp. 3155–3158, 2017.

[10] G. Ginestet et al., "Embroidered antenna-microchip interconnections and contour antennas in passive UHF RFID textile tags," *IEEE Antennas Wireless Propag. Lett.*, vol. 16, pp. 1205–1208, 2017.

[11] S. D. Keller et al., "Effects of metal nanoparticle doping and in situ atmospheric pressure plasma treatment on carbon nanotube sheet antenna performance," *IEEE Antennas Wireless Propag. Lett.*, vol. 16, pp. 1076–1079, 2017.

[12] J. Kumar, B. Basu, F. A. Talukdar, and A. Nandi, "Multimode-inspired low cross-polarization multiband antenna fabricated using graphene-based conductive ink," *IEEE Antennas Wireless Propag. Lett.*, vol. 17, no. 10, pp. 1861–1865, Oct. 2018.

[13] M. A. S. Tajin et al., "On the effect of sweat on sheet resistance of knitted conductive yarns in wearable antenna design," *IEEE Antennas Wireless Propag. Lett.*, vol. 19, no. 4, pp. 542–546, Apr. 2020.

[14] C. Hertleer, A. Tronquo, H. Rogier, L. Vallozzi, and L. Van Langenhove, "Aperture-coupled patch antenna for integration into wearable textile systems," *IEEE Antennas Wireless Propag. Lett.*, vol. 6, pp. 392–395, 2007.

[15] R. Aprilliyani, P. A. Dzagbletey, J. H. Lee, M. J. Jang, J. So, and J. Chung, "Effects of textile weaving and finishing processes on textile-based wearable patch antennas," *IEEE Access*, vol. 8, pp. 63295–63301, 2020.

[16] Y.-J. Chen, T.-W. Liu, and W.-H. Tu, "CPW-fed penta-band slot dipole antenna based on comb-like metal sheets," *IEEE Antennas Wireless Propag. Lett.*, vol. 16, pp. 202–205, 2017.

[17] B. K. Tehrani, B. S. Cook, and M. M. Tentzeris, "Inkjet printing of multilayer millimeter-wave yagi-uda antennas on flexible substrates," *IEEE Antennas Wireless Propag. Lett.*, vol. 15, pp. 143–146, 2016.

[18] Z. Wang et al., "High conductive graphene assembled films with porous micro-structure for freestanding and ultra-low power strain sensors," *Sci. Bull.*, vol. 65, no. 16, pp. 1363–1370, 2020.

[19] R. Song et al., "Wideband and low sidelobe graphene antenna array for 5G applications," *Sci. Bull.*, vol. 66, no. 2, pp. 103–106, 2021.

[20] R. Fang, R. Song, X. Zhao, Z. Wang, W. Qian, and D. He, "Compact and low-profile UWB antenna based on graphene-assembled films for wearable applications," *Sensors*, vol. 20, pp. 2552–2559, 2020.

[21] R. Song et al., "High-conductive graphene film based antenna array for 5G mobile communications," *Int. J. RF Microw. Comput.-Aided Eng.*, vol. 29, no. 6, 2019, Art. no. e21692.

[22] Z. Hu, Z. Xiao, S. Jiang, R. Song, and D. He, "A dual-band conformal antenna based on highly conductive graphene-assembled films for 5G WLAN applications," *Materials*, vol. 14, pp. 5087–5094, 2021.

[23] A. Y. I. Ashyap et al., "Fully fabric high impedance surface-enabled antenna for wearable medical applications," *IEEE Access*, vol. 9, pp. 6948–6960, 2021.

[24] A. Alemaryeen and S. Noghanian, "On-body low-profile textile antenna with artificial magnetic conductor," *IEEE Trans. Antennas Propag.*, vol. 67, no. 6, pp. 3649–3656, Jun. 2019.

[25] M. El Atrash, M. A. Abdalla, and H. M. Elhennawy, "A wearable dual-band low profile high gain low SAR antenna AMC-backed for WBAN applications," *IEEE Trans. Antennas Propag.*, vol. 67, no. 10, pp. 6378–6388, Oct. 2019.

[26] H.-R. Zu, B. Wu, Y.-H. Zhang, Y.-T. Zhao, R.-G. Song, and D.-P. He, "Circularly polarised wearable antenna with low profile and low specific absorption rate using highly conductive graphene film," *IEEE Antennas Wireless Propag. Lett.*, vol. 19, no. 12, pp. 2354–2358, Dec. 2020.

[27] R. Joshi et al., "Dual-band, dual-sense textile antenna with AMC backing for localization using GPS and WBAN/WLAN," *IEEE Access*, vol. 8, pp. 89468–89478, 2020.

[28] S. Li, R. Song, B. Zhang, B. Huang, X. Zhao, and D. He, "Wearable near-field communication bracelet based on highly conductive graphene-assembled films," *Int. J. RF Microw. Comput.-Aided Eng.*, vol. 31, pp. 2367–2374, 2021.

[29] R. Song et al., "Sandwiched graphene clad laminate: A binder-free flexible printed circuit board for 5G antenna application," *Adv. Eng. Mater.*, vol. 22, pp. 2000451–2000461, 2020.

[30] A. Y. I. Ashyap et al., "Robust and efficient integrated antenna with EBG-DGS enabled wide bandwidth for wearable medical device applications," *IEEE Access*, vol. 8, pp. 56346–56358, 2020.

[31] M. El Atrash, O. F. Abdalgalil, I. S. Mahmoud, M. A. Abdalla, and S. R. Zahran, "Wearable high gain low SAR antenna loaded with backed all-textile EBG for WBAN applications," *IET Microw.*, vol. 14, pp. 791–799, 2020.